Eur. Phys. J. D **17**, 189–204 (2001)

THE EUROPEAN PHYSICAL JOURNAL D

EDP Sciences

Radiative cooling of fullerene anions in a storage ring

J.U. Andersen[a], C. Gottrup, K. Hansen, P. Hvelplund, and M.O. Larsson

Institute of Physics and Astronomy, University of Aarhus, 8000 Aarhus, Denmark

Received 12 March 2001 and Received in final form 12 June 2001

Abstract. Thermionic emission from hot fullerene anions, C_N^-, has been measured in an electrostatic storage ring for even N values from 36 to 96. The decay is quenched by radiative cooling and hence the observations give information on the intensity of thermal radiation from fullerenes. The experiments are analysed by comparison with a simulation which includes the quantisation of photon energy and the statistics of emission. Experiments with heating of the molecules with a laser beam confirm the interpretation of the observations in terms of radiative cooling and give an independent estimate of the cooling rate for C_{60}^-. The measured cooling rates agree in general within a factor of two with the prediction from a classical dielectric model of a thermal radiation intensity of ~ 300 eV/s for C_{60} at 1 400 K, scaling approximately with the 6th power of the temperature and with the number of atoms in the molecule.

PACS. 36.40.-c Atomic and molecular clusters – 36.40.Cg Electronic and magnetic properties of clusters – 36.40.Qv Stability and fragmentation of clusters – 36.40.Wa Charged clusters – 39.10.+j Atomic and molecular beam sources and techniques

1 Introduction

Studies of the dynamics of fullerenes at high temperatures are important for the understanding of their formation and extraordinary stability [1,2]. The main decay channels for a highly excited fullerene molecule are emission of small clusters (mainly C_2) and electron emission. The key parameter in a statistical description is the energy barrier or activation energy for the decay. Most efforts have been devoted to studies of C_2 detachment, and there has been much controversy over the magnitude of the activation energy for this process [3–5]. Recently, it has been realised that radiative cooling of the hot fullerene molecules must be taken into account in the analysis of experiments, and attempts have been made to estimate the rate of this cooling from the experiments [4,6–9].

We have developed an alternative method for measuring the radiative cooling of hot fullerenes, in which the ambiguities involved in disentangling the interplay of two poorly known processes are avoided. The method is based on observation of the decay of fullerene anions in a storage ring [10–13]. The additional electron in the anions is bound by only about 3 eV [2], and hence electron emission dominates over C_2 detachment with a barrier of order 8–10 eV [8]. The emission is analogous to thermionic emission from a metal, and the rate constant is given by an expression similar to the Richardson-Dushman formula [11,14]. The electron affinities of the fullerenes are known fairly well [15] and the pre-exponential factor in the formula may be estimated *via* detailed balance from measured attachment cross-sections. It is therefore possible to simulate the observed decay rate as a function of time and extract the strength of radiative cooling as a function of their temperature [11].

The heating of molecules by photon absorption and competition between fragmentation and emission of photons from hot molecules has been studied extensively, in particular by Dunbar's group (see, for example, Refs. [16–19]). This work has focussed on the interaction of molecules with infrared radiation, which is dominated by the molecular vibrations, but an extension to higher temperatures, where electronic degrees of freedom dominate the cooling, was reported in reference [20]. Continuous, black-body like emission spectra have been recorded both for very hot fullerenes [21] and for metal clusters [22]. It is difficult, however, to draw conclusions on the emission intensity from the observed spectra; for example, there can be additional cooling by particle emission [22]. Direct quantitative evidence for radiative cooling was obtained in an experiment with V_{13}^+ clusters in an ion trap [23], from the dependence of the fragmentation yield on the delay between two laser pulses exciting the ions. The measured cooling rates were found to be in fairly good agreement with calculations based on the Mie theory for absorption of radiation from small particles [24,25], with the bulk dielectric function for vanadium.

Similar calculations have been carried out for radiation from fullerenes. However, these molecules consist of a single shell of atoms, and a quantitative description cannot be obtained with a bulk dielectric function, for example from graphite (see Appendix C of Ref. [26]). Also calculations based on measured absorption cross-sections [20,27] are

[a] e-mail: jua@ifa.au.dk

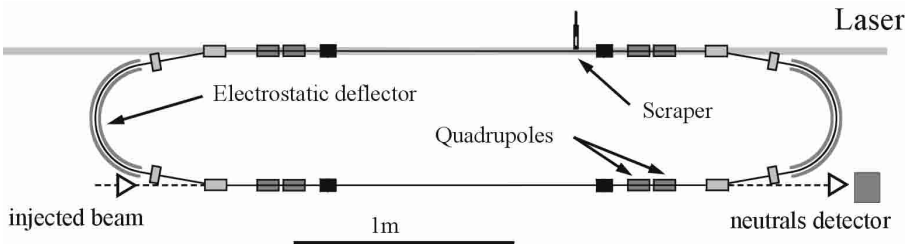

Fig. 1. Schematic layout of the electrostatic storage ring ELISA.

unreliable because the strength and width of absorption lines depend strongly on temperature [28]. As an alternative, a classical dielectric model has been developed, with parameters adjusted to reproduce the main features of the available experimental results on the absorption of electromagnetic radiation by fullerenes, in the gas phase, in solution, and in solid films [26,28]. Through detailed balance, the model then provides a quantitative prediction of the intensity of radiation from fullerenes, as a function of the internal temperature and of the number of atoms in the molecule [26].

Here we report on an extension of the measurements of cooling of hot fullerenes, with the aim of testing the predictions from this model. We have mainly used a newly constructed storage ring, ELISA (ELectrostatic Ion Storage ring, Aarhus), which has made it possible to study fullerene anions, C_N^-, with even N values from 36 to 96. Also the analysis of the measurements has been improved. An important simplifying approximation was the treatment of radiative cooling as a continuous process [11]. We have now developed simulations based on the master equation, in which the quantisation of photon energy and the statistics of the emission process are taken into account. The calculations are similar to simulations applied earlier by Dunbar and others in the study of radiative heating and cooling of molecules [16–20]. As a supplement, we have tested the interpretation of the experiments by introducing heating due to absorption of photons from a laser.

In the following, we first describe the experimental details with examples of the measured spectra. We then discuss in some detail the physical interpretation of the results and the simulations applied to derive the rate of radiative cooling from the measurements. Brief theoretical discussions of thermionic emission and thermal radiation are given in Appendices A and B. Finally the data are presented together with fits by simulations, and the derived cooling rates are compared with the predictions from the dielectric model. An attempt at a more detailed analysis of the radiation from the magic fullerenes, $N = 50$, 60 and 70, based on measured energies and strengths of radiative transitions, is described in Appendix C. In particular, the role played by the additional electron in the anions is analysed.

2 Experiments

The experiments have been carried out at the ion storage rings in Aarhus [29]. The small, purely electrostatic ring ELISA is illustrated in Figure 1 [30]. In the ion source, fullerene molecules exit from an oven into a plasma created by electron bombardment of the support gas (normally nitrogen). Both negative and positive ions are formed and the source can deliver nanoampere currents of C_{60} and C_{70} ions. The fullerene powder contains small amounts of heavier fullerenes, and lighter fullerenes are created by C_2 emission in the hot plasma. Only fullerene ions with an even number of atoms are formed with sufficient intensity ($> 10^{-11}$ A). The ions are extracted and accelerated to 22 keV and are then mass selected by a magnet.

At the beginning of each cycle of the measurement, a new bunch of ions is injected and stored in the ring while the previously stored ions are dumped. It is a great advantage of the electrostatic ring that the ring parameters can be left untouched when ions with a different mass are injected. This makes it possible to store very weak beams, and we have made measurements on fullerene anions with even numbers of atoms from 36 to 96. Electron detachment from stored ions is monitored by detection of neutral molecules with a channel-plate detector in a corner of the ring. The secondary electrons generate a light pulse from a fluorescent screen and, in addition to the electronic counting, the distribution of the pulses over the detector area (~ 12 cm^2) is recorded with a camera and displayed live. The divergence of the beam is small enough that the pulses from the molecules neutralised by electron emission are focussed in the central area of the detector. There is also nearly complete collection of neutrals formed by collisions because the dominant rest gas is hydrogen which has a very small mass compared to the fullerenes. The same type of detector was used at ASTRID (Aarhus STorage RIng, Denmark), but owing to the larger circumference (~ 40 m) of this ring, the average distance from the region of decay to the detector is larger (~ 6 m compared to ~ 2 m). Furthermore, the beam size and divergence in ASTRID are larger than in ELISA. Hence the collection of neutrals is incomplete, and oscillations of the yield with time, associated with betatron oscillations of the beam, are often observed. The necessity to average over such oscillations contributes to the poorer time resolution of measurements at ASTRID compared to those at ELISA.

The counts in the neutrals detector were stored in a multichannel spectrum, with the channel number representing the time after injection, and counts were accumulated with the maximum injection rate allowed by the desired length of the spectrum. To avoid a dependence of the spectral shape on beam current it was found necessary to limit the current in ASTRID to give a count rate of less

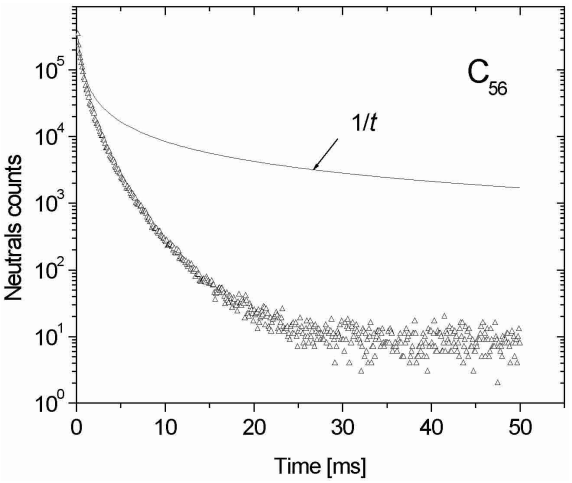

Fig. 2. Time spectrum of neutrals counts for a stored C_{56}^- beam in ELISA, compared with a $1/t$ distribution.

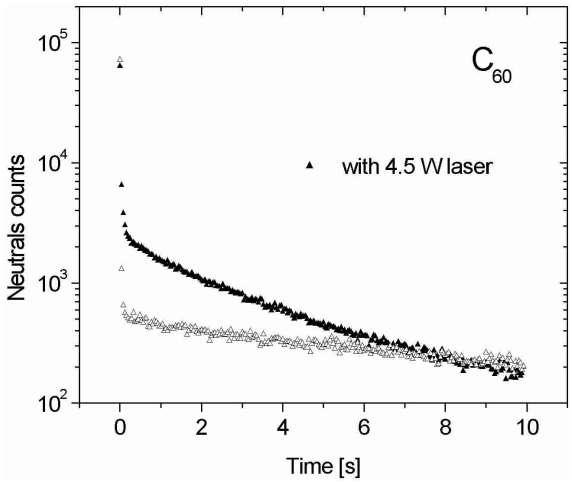

Fig. 3. Time spectrum of neutrals counts for a stored C_{60}^- beam in ELISA, with and without irradiation by a 4.5 W CW Nd:YAG laser. Each point corresponds to a 40 ms interval.

than 30 kHz just after injection. The dependence of the spectrum on beam current at higher count rates seemed to be due to a pressure transient in the ring, caused presumably by the high flux of neutral molecules hitting the walls in the vacuum tubes just after injection. Detector saturation effects were only observed for at least an order of magnitude higher count rates. We have applied the same restriction to the currents stored in ELISA.

A typical spectrum is illustrated in Figure 2. The time resolution of the experiment is the revolution time, which is about 100 μs in ELISA and a factor of four longer for 45 keV fullerene ions in ASTRID. Each point in the figure corresponds to an integral over one revolution time. At short times, $t < 20$ ms, there is a very high rate of neutrals, which we interpret as thermionic emission from hot molecules [11]. The rapid decrease of this signal carries information about radiative cooling. At longer times, the stored current is reduced exponentially due to collisions with rest gas molecules, and with pressures of a few times 10^{-11} mbar the lifetime is of order 10 s. For the shortest times, $t < 1$ ms, the decrease of the yield is due to depletion of the hottest molecules, and as discussed below (see also Refs. [11,13]), the time dependence is expected to be close to a $1/t$ distribution, where t is the time after creation of the ensemble of isolated hot molecules. We have observed that this part of the spectrum depends on the parameters of the plasma ion source, in particular on the anode voltage. The dependence can be accounted for by introduction of a contribution to t from a delay Δt of a few hundred microseconds inside the source. A plausible explanation is that the heating by bombardment with energetic electrons is weak near the exit aperture, and that the delay corresponds to an ion diffusion time in the plasma. The delay can be reduced and nearly eliminated by an increase of the anode voltage. For the measurements shown in Figure 2 the delay is found to be $\Delta t \sim 100$ μs, only.

As illustrated in Figure 1, the beam from a laser can be used to heat the molecules in one side of the ring. Such measurements provide a test of the interpretation of the measurements in terms of radiative cooling, and they can also give an independent check of the measured cooling rates. We have carried out experiments with both pulsed and CW laser beams. The measurements with a CW laser were performed at ASTRID with a set-up similar to the one shown in Figure 1. With a small moveable plate blocking the beam from a Nd:YAG laser, the irradiation could be switched on and off at well defined times after injection of the ion beam, with a rise time of about 1 ms. One example is illustrated in Figure 3. Here the stored C_{60}^- beam was illuminated continuously with a 4.5 W laser beam. Initially, the cooling of very hot molecules dominates and the yield decreases rapidly, but after a few hundred milliseconds an equilibrium between cooling and heating is established, leading to an exponential decay of the beam by electron emission with a life time much shorter than the collision lifetime. The small curvature in the logarithmic plot can be explained by incomplete overlap of the laser beam with the ion beam. Owing to the larger dimensions of ASTRID and the larger beam size, it is more difficult to optimise the overlap in this ring. Even when averaged over many revolutions, the overlap can be quite different for ions with large and small amplitudes in the betatron oscillations around the central trajectory in the ring. However, the non-uniformity of the illumination can be taken into account in the analysis, as discussed in Section 5. The measurements with a CW laser give a detailed test of the interpretation of the observations in terms of radiative cooling, but it is difficult to obtain quantitative estimates of the cooling rates from these measurements because the absorption cross-section is poorly known.

At ELISA we have used a pulsed OPO (Optical Parametric Oscillator) laser with variable wavelength and 10 Hz repetition rate. The laser was synchronised with the injection of ions into the ring, with a variable delay. We shall in Section 5 analyse a measurement with heating at 30.3 ms by a 2 mJ pulse of 1.2 eV photons. The counts

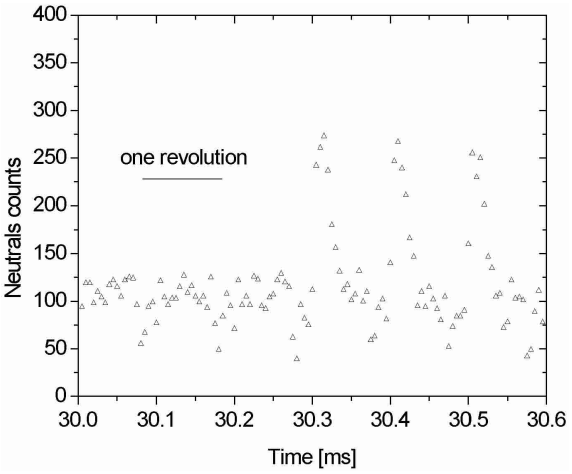

Fig. 4. Section of a time spectrum for C_{60}^- stored in ELISA and exposed at ~ 30.3 ms after injection to a 2 mJ laser pulse with 1.2 eV photon energy. The points correspond to 5 μs intervals and the revolution time is about 100 μs.

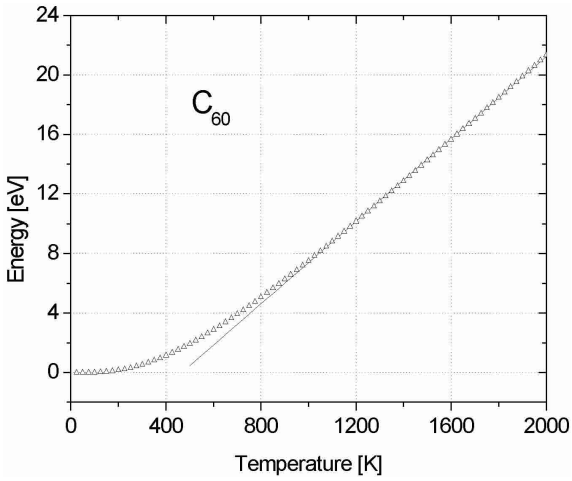

Fig. 5. Heat capacity of C_{60}, calculated as described in reference [11] The line is from a linear fit in the range 1 000–2 000 K, as given in equation (1).

of neutrals over six revolutions of a stored C_{60}^- beam near this time are shown in Figure 4. The stored ion pulse fills 93% of the circumference of the ring, and the plateaus of counts from one revolution are separated by a narrow dip. After the laser pulse, the count rate is enhanced by about a factor of two for the ions hit by the laser, and this increase is seen each time the hot molecules pass in front of the detector. The heated molecules cool faster, and hence the enhancement of the yield decreases with the storage time after the laser pulse. As we shall show in Section 5, it is possible from the observed rate of decrease to derive an independent estimate of the cooling rate.

3 Depletion and cooling

There is good evidence for the interpretation of electron emission from fullerene anions as a statistical process (Appendix A). A statistical equilibrium of an isolated molecule can be represented by a microcanonical ensemble of molecules with fixed excitation energy E, and a microcanonical temperature may be introduced, defined by the relation $1/k_{\mathrm{B}}T = \mathrm{d}/\mathrm{d}E\rho(E)$, where $\rho(E)$ is the level density and k_{B} Boltzmann's constant [31]. For the large fullerene molecules, it can with sufficient accuracy be calculated as the temperature T of a canonical ensemble with average excitation energy equal to E. Even at excitation energies of 10–20 eV, the range relevant for our experiments, the temperature is moderate and hence nearly all the energy resides in vibrations. The connection between temperature and average excitation energy for C_{60} was calculated as described in reference [11], and as illustrated in Figure 5 it may between 1 000 K and 2 000 K be approximated by the linear expression

$$E[\mathrm{eV}] = 7.4 + 0.0138(T[\mathrm{K}] - 1\,000). \qquad (1)$$

The heat capacity, $C = 0.0138$ eV/K, corresponds to the high-temperature limit for ~ 160 harmonic oscillators, which is $\sim 8\%$ less than the total number of internal degrees of freedom, $3N - 6$ for C_N. For the other fullerenes, we scale the expression in equation (1) by a factor $(3N - 6)/174$.

In the plasma ion source the ions are bombarded with electrons and we expect the fullerene ions to emerge highly excited and with a broad distribution in temperature. This is supported by our observation of decay in ELISA of fullerene cations injected from the same source, indicating that the distribution for these ions extends to $T \sim 3\,000$ K [32]. After exit from the source, the distribution in temperature of the anions is modified by depletion due to thermionic emission and by cooling due to emission of photons. Let us first disregard radiative cooling. The time dependence of the distribution is then given by

$$-\frac{\partial}{\partial t} g(T_{\mathrm{e}}, t) = k(T_{\mathrm{e}}) g(T_{\mathrm{e}}, t), \qquad (2)$$

where k is given by equations (A.2, A.3), and where, for simplicity, the distribution in excitation energy is expressed as a function of the emission temperature T_{e}. The total rate of electron emission at time t is then obtained as

$$I_{\mathrm{e}}(t) = \int \mathrm{d}T_{\mathrm{e}} k(T_{\mathrm{e}}) \exp\left(-k(T_{\mathrm{e}})t\right) g(T_{\mathrm{e}}, 0). \qquad (3)$$

The weight function multiplying the initial distribution, $g(T_{\mathrm{e}}, 0)$, has a sharp maximum. From differentiation we find that the rate constant is $k_{\mathrm{m}} = t^{-1}$ at the maximum, and from the Arrhenius expression in equation (A.2) we obtain for the corresponding emission temperature,

$$T_{\mathrm{m}}(t) = E_{\mathrm{b}}/G_{\mathrm{m}}k_{\mathrm{B}}, \text{ with } G_{\mathrm{m}} = \ln(\nu t). \qquad (4)$$

We have denoted the magnitude of the exponent in equation (A.2) by G since this quantity is usually called the Gspann parameter in statistical analysis of cluster dynamics. With the frequency ν given in Appendix A, we obtain $G_{\mathrm{m}} \simeq 23$ in the time range of a few ms for decay

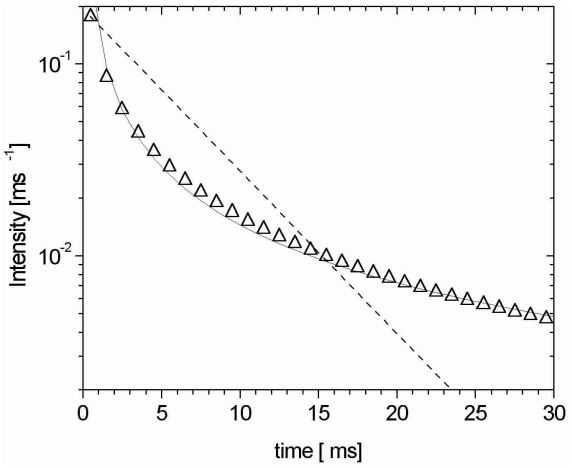

Fig. 6. Intensity of electron emission from C_{60}^- ions leaving at $t = 0$ an oven at 1 300 K. The triangles give the results of a calculation based on equations (3, A.2, A.3), with an energy distribution normalised at $t = 0$ and with the decay parameters discussed in Appendix A. The solid curve illustrates a $1/t$ dependence and the dashed curve gives the intensity for decay in thermal equilibrium at 1 300 K.

of C_{60}^-, and the temperature at the maximum becomes $T_\mathrm{m} \approx 1\,300$ K. The weight function multiplying $g(T_\mathrm{e}, 0)$ in the integral in equation (3) may be approximated by a Gaussian, centred at T_m and with a width given by

$$\sigma = \left(\frac{\mathrm{d}}{\mathrm{d}T_\mathrm{m}} \ln k(T_\mathrm{m})\right)^{-1} \simeq \frac{E_\mathrm{b}}{k_\mathrm{B} G_\mathrm{m}^2}\,. \tag{5}$$

If $g(T_\mathrm{e}, 0)$ varies slowly with temperature, it may be taken outside the integral and we then obtain

$$I_\mathrm{e}(t) \simeq \frac{1}{t}\frac{E_\mathrm{b}}{k_\mathrm{B} G_\mathrm{m}^2} g(T_\mathrm{m}, 0), \tag{6}$$

where we have omitted a factor $\sqrt{2\pi}\mathrm{e}^{-1} \simeq 1$. Since G_m varies only slowly with time, the decay rate is nearly proportional to t^{-1} [6,11,13,33].

It is interesting that the width of the region contributing effectively to the decay rate is quite narrow, $2\sigma/T_\mathrm{m} \simeq 2G_\mathrm{m}^{-1} < 10\%$, narrower by more than a factor of two than the width of a canonical distribution. This suggests that thermionic emission may be used to select an ensemble of molecules with quite well defined excitation energy. The calculation shown in Figure 6 illustrates that the canonical energy distribution is quite broad in this context. The rate of electron emission has been calculated for C_{60}^- molecules leaving at time $t = 0$ an oven at temperature 1 300 K. Owing to the depletion from the high-energy side, the rate is highly non-exponential and much closer to a $1/t$ distribution.

In view of the expected t^{-1} scaling, our observation of a nearly exponential decay with lifetimes of the order of a few milliseconds for fullerene anions stored in ASTRID gave strong evidence for quenching of the electron emission by radiative cooling [11]. We first, as before, treat the radiative cooling as a continuous process without quantisation of the photon energy. The temperature of the molecules is now a function of time but it is convenient to keep their initial emission temperature T_i as the variable in the distribution and to describe the radiative cooling by a separate function, $T_\mathrm{e}(T_\mathrm{i}, t)$ [34]. The development with time of this function and of the distribution $h(T_\mathrm{i}, t)$ is then governed by two coupled equations,

$$\begin{aligned} -\frac{\partial}{\partial t} T_\mathrm{e}(T_\mathrm{i}, t) &= I_\mathrm{r}(T_\mathrm{e})/C \\ -\frac{\partial}{\partial t} h(T_\mathrm{i}, t) &= k(T_\mathrm{e}) h(T_\mathrm{i}, t), \end{aligned} \tag{7}$$

with k given by equations (A.2, A.3) and with $I_\mathrm{r}(T_\mathrm{e})$ denoting the radiation power. If it is proportional to some power of the emission temperature,

$$I_\mathrm{r}(T_\mathrm{e}) = C\gamma T_\mathrm{e}^n, \tag{8}$$

we obtain an analytical solution for the time dependence of the emission temperature [4],

$$T_\mathrm{e}(T_\mathrm{i}, t) = \left(T_\mathrm{i}^{-(n-1)} + (n-1)\gamma t\right)^{\frac{-1}{n-1}}. \tag{9}$$

It is very instructive to consider the case $n = 2$, for which the equations (7) have analytical solutions,

$$\begin{aligned} T_\mathrm{e}(T_\mathrm{i}, t)^{-1} &= T_\mathrm{i}^{-1} + \gamma t \\ h(T_\mathrm{i}, t) &= h(T_\mathrm{i}, 0) \exp\left(-\nu \mathrm{e}^{-E_\mathrm{b}/k_\mathrm{B}T_\mathrm{i}} (1 - \mathrm{e}^{-\alpha t})/\alpha\right), \end{aligned} \tag{10}$$

with $\alpha = \gamma E_\mathrm{b}/k_\mathrm{B}$. We now insert these formulas into the analogue of equation (3),

$$\begin{aligned} I_\mathrm{e}(t) &= \int \mathrm{d}T_\mathrm{i} k(T_\mathrm{e}(T_\mathrm{i}, t)) h(T_\mathrm{i}, t) \\ &= \int \mathrm{d}T_\mathrm{i} \nu \mathrm{e}^{-E_\mathrm{b}/k_\mathrm{B}T_\mathrm{i}} \mathrm{e}^{-\alpha t} \\ &\quad \times \exp\left(-\nu \mathrm{e}^{-E_\mathrm{b}/k_\mathrm{B}T_\mathrm{i}} (1 - \mathrm{e}^{-\alpha t})/\alpha\right) h(T_\mathrm{i}, 0). \end{aligned} \tag{11}$$

After extraction of a factor $\alpha/(\exp(\alpha t) - 1)$, the integral has the same form as before, and the result can be obtained from equations (4, 6) with the replacements $\nu t \to \nu(1 - \mathrm{e}^{-\alpha t})/\alpha$ and $t^{-1} \to \alpha/(\mathrm{e}^{\alpha t} - 1)$, *i.e.*,

$$\begin{aligned} T_\mathrm{i,m}(t) &= \frac{E_\mathrm{b}}{k_\mathrm{B} G_\mathrm{m}}, \\ I_\mathrm{e}(t) &\simeq \frac{\alpha}{\mathrm{e}^{\alpha t} - 1} \frac{E_\mathrm{b}}{k_\mathrm{B} G_\mathrm{m}^2} h(T_\mathrm{i,m}, 0), \\ \text{with } \; G_\mathrm{m} &= \ln\left(\nu(1 - \mathrm{e}^{-\alpha t})/\alpha\right). \end{aligned} \tag{12}$$

At short times the rate is unchanged, $I_\mathrm{e} \propto t^{-1}$, but the decay is quenched exponentially, $I_\mathrm{e} \propto \exp(-\alpha t)$, after a characteristic time $\tau_\mathrm{c} = \alpha^{-1}$. According to equation (8), τ_c is given in terms of the cooling rate by the relation

$$\tau_\mathrm{c}^{-1} = -G \frac{\mathrm{d}}{\mathrm{d}t} \ln T_\mathrm{e}. \tag{13}$$

When the rapid depletion stops, the initial temperature corresponding to the maximum of the weight function in

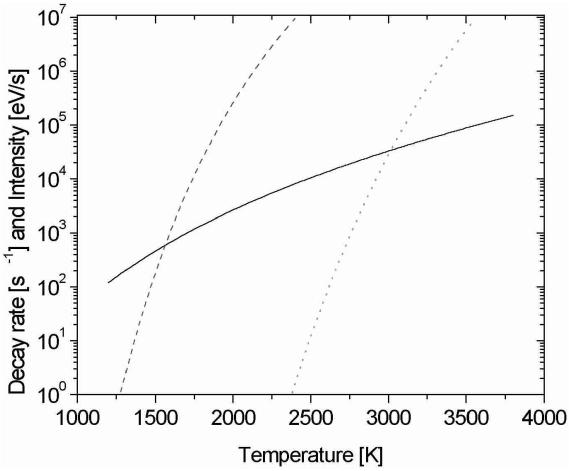

Fig. 7. Decay rates for electron emission from C_{60}^- (dashed) and C_2 emission from C_{60} (dotted) compared with the radiation intensity obtained from the dielectric model (full). From reference [26], Figure 7.

equation (11) approaches the value

$$T_c = E_b/G_c k_B, \tag{14}$$

where $G_c = \ln(\nu\tau_c)$.

For higher powers n, for example $n \simeq 6$ as in the dielectric model discussed in Appendix B, a similar result is obtained, with a characteristic time determined from equation (13) evaluated at $t = \tau_c$ and $T_e = T_c$. This can be understood qualitatively from the comparison in Figure 7 of the radiation intensity, as predicted from the dielectric model, with the rate of electron emission according to equation (A.2). The characteristic temperature T_c is close to the crossing of the two curves [26], and cooling dominates for $T < T_c$. This temperature is reached at $t \sim \tau_c$ when hotter molecules have decayed, and for $t > \tau_c$ the rate of electron emission is reduced by cooling according to equations (9, A.2). An approximate analytical extrapolation to the region $t < \tau_c$ was given in reference [11]. The most important difference from equation (12) is that the function $\ln(I_e(t))$ has a curvature for $t \gg \tau_c$, which is positive for $n > 2$ and increases with n. The measured curvature of this function therefore gives information about the temperature dependence of the radiation intensity.

4 Discrete model

In this section we describe simulations which include the quantisation of the emitted radiation. Simulations based on a master equations have a broad applicability in physics [35]. The calculations described in the following were based on methods we had developed in a different context [36]. Similar simulations have been applied earlier in the analysis of experiments involving radiative cooling of molecules [16–20].

It is convenient for numerical evaluation to formulate the description in discrete notation. We now again use the emission temperature in equation (A.3) as the variable and divide the temperature scale into intervals ΔT with midpoint T_j. The distribution over T_e at time t is expressed as a vector $\{g_j(t)\}$, where the element g_j is the number of molecules in the jth interval. The rate may then in analogy to equation (3) be written as

$$I_e(t) = \sum_j k(T_j) g_j(t). \tag{15}$$

The continuous cooling of the distribution is replaced by probabilities $W_{ij}\mathrm{d}t$ of transitions from T_j to T_i. The transition strengths are obtained from equation (B.1) with the model cross-section $\sigma(\omega) \propto \omega^2$,

$$W_{ij} \;\propto\; (j-i)^4 \left(\exp\left[\frac{(j-i)C\Delta T}{k_B(T_j - (j-i)\Delta T/2)} \right] - 1 \right)^{-1}, \tag{16}$$

for $T_j > T_i$. The constant of proportionality is varied to fit a measurement, and the resulting value of the radiation intensity is the principal results of the experiment. For emission of radiation W_{ij} is zero for $T_i > T_j$, but the formalism can also describe absorption of photons with energy $\hbar\omega$ by inclusion of off-diagonal matrix elements for $(i-j)C\Delta T = \hbar\omega$. A temperature dependence of the absorption cross-section can be represented by a j-dependence of the magnitude of this matrix element.

The matrix $A_{ij}(\mathrm{d}t)$ which propagates the distribution from t to $t + \mathrm{d}t$,

$$g_i(t + \mathrm{d}t) = \sum_j A_{ij}(\mathrm{d}t) g_j(t), \tag{17}$$

includes depletion in the diagonal,

$$A_{ij}(\mathrm{d}t) = \begin{cases} W_{ij}\mathrm{d}t \;\text{ for }\; i \neq j \\ 1 - (\sum_n W_{nj} + k(T_j) + 1/\tau)\,\mathrm{d}t \;\text{ for }\; i = j \end{cases}. \tag{18}$$

The three terms in the parenthesis represent radiative cooling (and heating), thermionic emission, and electron detachment in collisions with rest-gas molecules. We assume the cross-section for the latter process to be independent of temperature (it is roughly geometric [37]) and τ is then the measured lifetime at long times, where thermionic emission is negligible.

The main problem in the numerical evaluation is the choice of the magnitude of the temperature interval ΔT. With decreasing ΔT, the size of the matrices increases and the computing time increases rapidly. However, we have found that usually ΔT can be chosen as large as 20 K without significant loss of accuracy. For a given value of ΔT, the basic time interval $\mathrm{d}t$ must be chosen small enough for the diagonal elements to be close to unity in the relevant temperature range. This, in contrast, represents no computational problem because the propagator from $t = 0$ to

a final time t can be evaluated by matrix multiplication in geometric progression,

$$A_{ij}(2^n \mathrm{d}t) = \sum_n A_{in}(2^{n-1}\mathrm{d}t)A_{nj}(2^{n-1}\mathrm{d}t), \quad n = 1, 2, 3, ... \quad (19)$$

Only ten steps are required to calculate a propagator to milliseconds when dt is of the order microseconds, and reduction of dt by a factor of two adds only one extra step.

The accuracy of the continuum approximation in equation (7) depends on the magnitude of the photon energies. To estimate the accuracy, we consider the change in the emission rate due to cooling alone. From equations (15, 17, 18) we find

$$\left(\frac{\mathrm{d}}{\mathrm{d}t}I_\mathrm{e}(t)\right)_\mathrm{rad} = \sum_{i,j} k(T_i)\left(W_{ij}g_j(t) - W_{ji}g_i(t)\right) = \sum_{i,j}\left(k(T_i) - k(T_j)\right)W_{ij}g_j(t). \quad (20)$$

We expand the change in the rate constant to second order in the temperature change $T_i - T_j = -(j-i)\Delta T$ after emission of a photon with energy $C(j-i)\Delta T = \hbar\omega$,

$$k(T_\mathrm{e} - (j-i)\Delta T) - k(T_\mathrm{e}) \simeq -(j-i)\Delta T k'(T_\mathrm{e}) + 1/2(j-i)^2\Delta T^2 k''(T_\mathrm{e}), \quad (21)$$

where $k(T_\mathrm{e})$ is given by equation (A.2). When only the first-order term is retained we obtain from equation (20)

$$\left(\frac{\mathrm{d}}{\mathrm{d}t}I_\mathrm{e}(t)\right)_\mathrm{rad} = \sum_j -(I_\mathrm{r}(T_j)/C)k'(T_j)g_j(t), \quad (22)$$

where $I_\mathrm{r}(T_j)$ is the radiation power at temperature T_j. This formula is equivalent to the result obtained from the continuum approximation (first lines in Eqs. (7, 11)). The relative magnitude of the second-order term in equation (21) is therefore a measure of the deviation from the continuum model, and the condition for applicability of this model may be expressed as

$$\hbar\omega < 2(CT_\mathrm{e})/G. \quad (23)$$

For $T_\mathrm{e} = 1\,200$ K, the right-hand side is about 1 eV. When photon energies of this magnitude are important, the continuum description is not sufficiently accurate. The second derivative of k is positive, and it is seen that the correction term reduces the effect of radiation on the decay rate. Fits to experiments with the continuum approximation for the radiative cooling therefore lead to underestimates of the radiation power. As indicated by equation (23), the error is largest for the smaller fullerenes, and with the photon energy spectrum predicted by the dielectric model the error varies from $\sim 30\%$ for $N = 36$ to less than 10% for $N = 96$. However, the error can be larger when discrete emission lines are included, like the 1.15 eV line for C_{60}^-.

5 Results and discussion

We now present experimental results together with the curves obtained from simulations, and typical examples are shown in Figure 8. The initial distribution in temperature was chosen as a Gaussian with maximum at 2 000 K and a width ~ 450 K, which was varied slightly (typically within $\pm 10\%$) to optimise the fit. The role of the width parameter is to determine the fall-off of the distribution towards low temperatures. The measured quantity which depends on this fall-off is the ratio between the intensities at short and at long times, since the rate of thermionic emission at short times is proportional to the value of the distribution at high temperatures while the rate of collisional detachment dominating the yield at later times is proportional to the integral of the (depleted) distribution.

The earliest part of the decay curve is determined by depletion and should be close to a $1/t$ distribution, as discussed in Section 3. As mentioned in Section 2, we have found it necessary to include a delay of typically a few hundred microseconds in the ion source to reproduce the observations in this depletion region by simulation. However, this does not have much influence on the derivation of a radiation intensity from the measurements. In the simulations, an electronic radiation intensity proportional to T^6 was used, with the absolute power adjusted to fit the experiments. The strength of the radiation is determined by the characteristic time scale for the decrease of the neutrals yield by orders of magnitude below the $1/t$ curve (see Fig. 2), according to equation (13). The sensitivity of the calculated curves to the cooling power and to its dependence on temperature is illustrated in Figures 9e and 9f. We see that the high quality of the fits to experiments in Figures 8 and 9 implies that the temperature dependence of the radiation intensity is close to the sixth power of T, as predicted by the dielectric model.

Figures 9a–9d show the results for the four magic molecules [1] with $N = 36$, 50, 60, and 70. For $N = 50$ and 60 the cooling is clearly slower than for the others, but this is not the case for $N = 36$ and 70 (see also Fig. 10). This observation correlates with the details of the absorption spectrum discussed in Appendix B: among the magic molecules, the HOMO-LUMO gap for the neutral molecule is largest for C_{60} (~ 1.7 eV), somewhat smaller for C_{70} (~ 1.3 eV) and for C_{50} (~ 1 eV) [38], and probably smallest for C_{36} [39]. However, the strength of the cooling does not follow this order since there is a strong transition in the gap for the additional electron in the anions of the first two molecules. The contribution to radiative cooling from this electron should be largest for C_{70}^-, where the transition energy is lowest. It may also play a role that there are more infrared-active vibrations for this molecule [26].

The cooling powers obtained from fits to measurements of the type illustrated in Figures 8 and 9 are shown in Figure 10. The first observation is that nearly all the points agree with the model prediction within a factor of two. The experimental points scatter around the prediction but appear to be systematically higher for large N. A main source of error in the experiments is the uncertainty

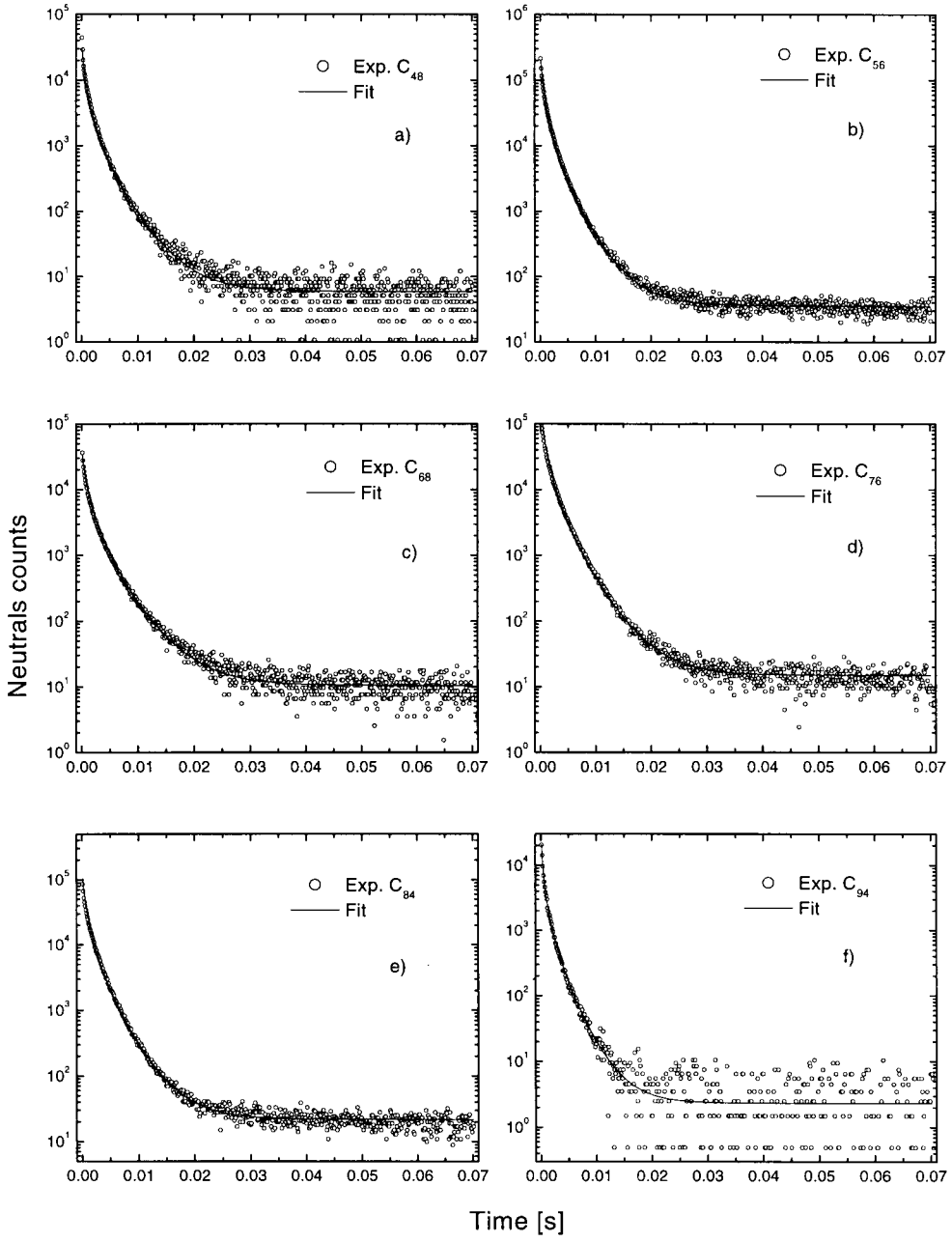

Fig. 8. Typical time spectra of the neutrals yield from stored non-magic fullerene anions, compared with simulations. The radiation power was varied to fit the experiments, and the results are given in Figure 10.

of the electron affinity E_b. With the assumption that the radiation intensity scales as the 6th power of T, the intensity derived from the analysis is proportional to E_b^{-5}. A typical uncertainty of 5% on the electron affinity therefore leads to 25% uncertainty in the radiation intensity. This dependence is illustrated by the alternative analysis for a few fullerenes with the electron affinity reduced by $\sim 10\%$, as discussed in Section 3. The pre-exponential factor ν in equation (A.2) is a less important parameter because it only enters the formula for the temperature inside a logarithm (Eq. (14)). Thus a change of ν by a factor of two leads to changes of only about 10% in the radiation intensities in Figure 10. The uncertainty from experimental sources of error can be estimated from the reproducibility of the results. Many of the spectra have been recorded several times under different experimental conditions. Typically, the derived cooling power does not vary by more than about 10% but differences as large as 25% have been obtained in a few cases. Altogether, the uncertainties should not be larger than 30–50%.

For hot C_{60}^- molecules, the single-electron transition at 1.15 eV dominates the absorption below about 1.5 eV [38,40–43], and this line should therefore also dominate the radiation intensity. In an alternative analysis, we have simulated the measured decay spectrum in Figure 9c with a heat radiation composed of two lines, one at 1.15 eV and the other at 0.25 eV, and with a temperature dependence given by equation (B.1). From the fit to the measurement we obtain line intensities of 400 eV/s and 60 eV/s at 1 500 K. As shown in Appendix C, the

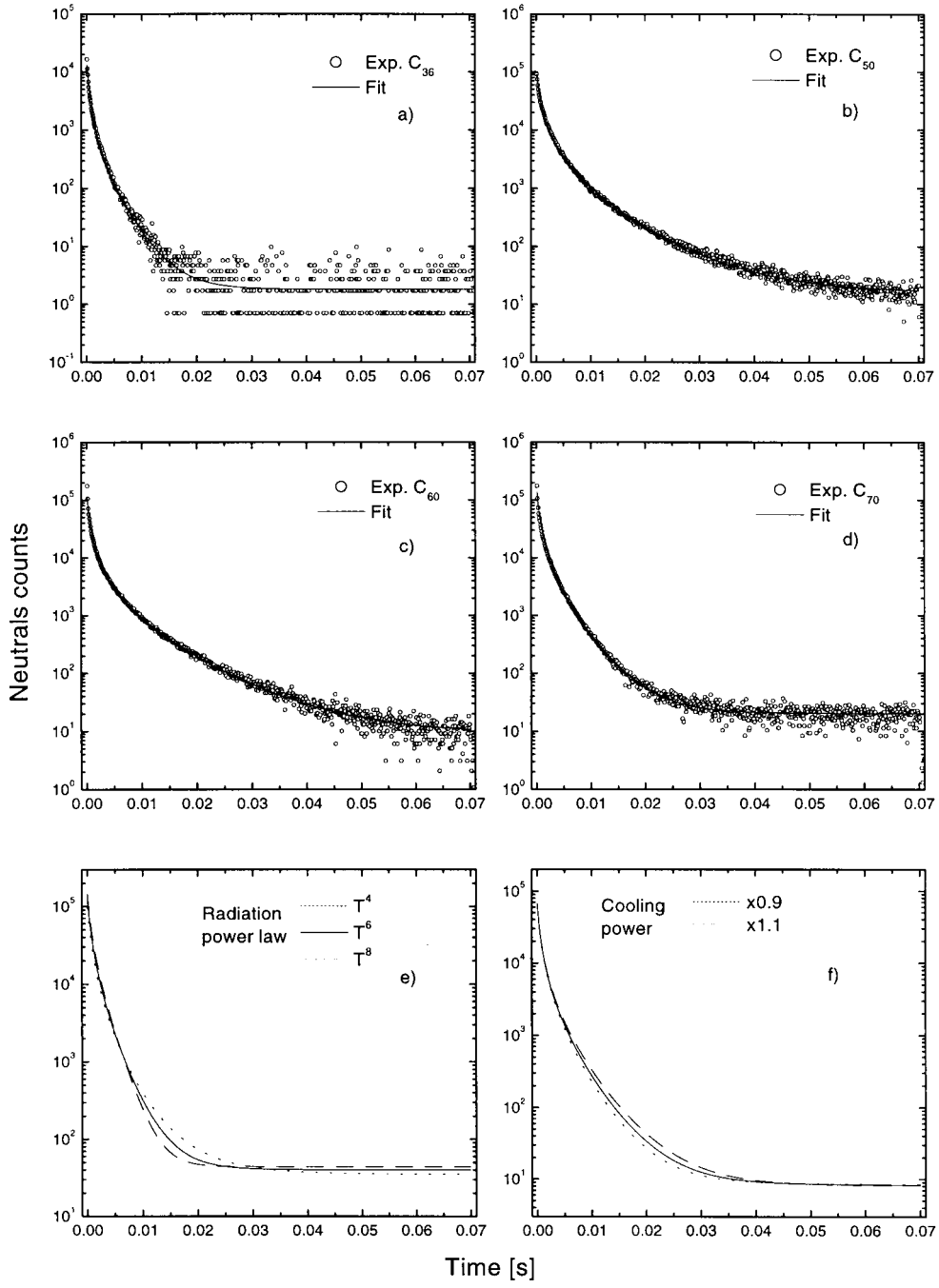

Fig. 9. As Figure 8 but for the magic fullerene anions C_N^-, $N =$ 36, 50, 60, and 70. The two lower curves illustrate the sensitivity of the simulations to a variation of the cooling power and its temperature dependence.

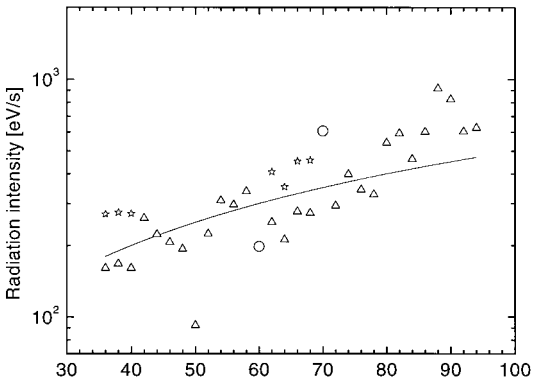

Fig. 10. Radiation intensity at 1 400 K for fullerene anions C_N^-, derived from fits to the measurements as illustrated in Figures 8 and 9. The results are compared with the prediction from a classical dielectric model [26]. The different symbols correspond to different values of the electron affinity. For C_{60} and C_{70} an electron affinity of 2.67 eV was used, and for all the other fullerenes 3.15 eV. The stars indicate radiation intensities derived with the alternative value of 2.85 eV.

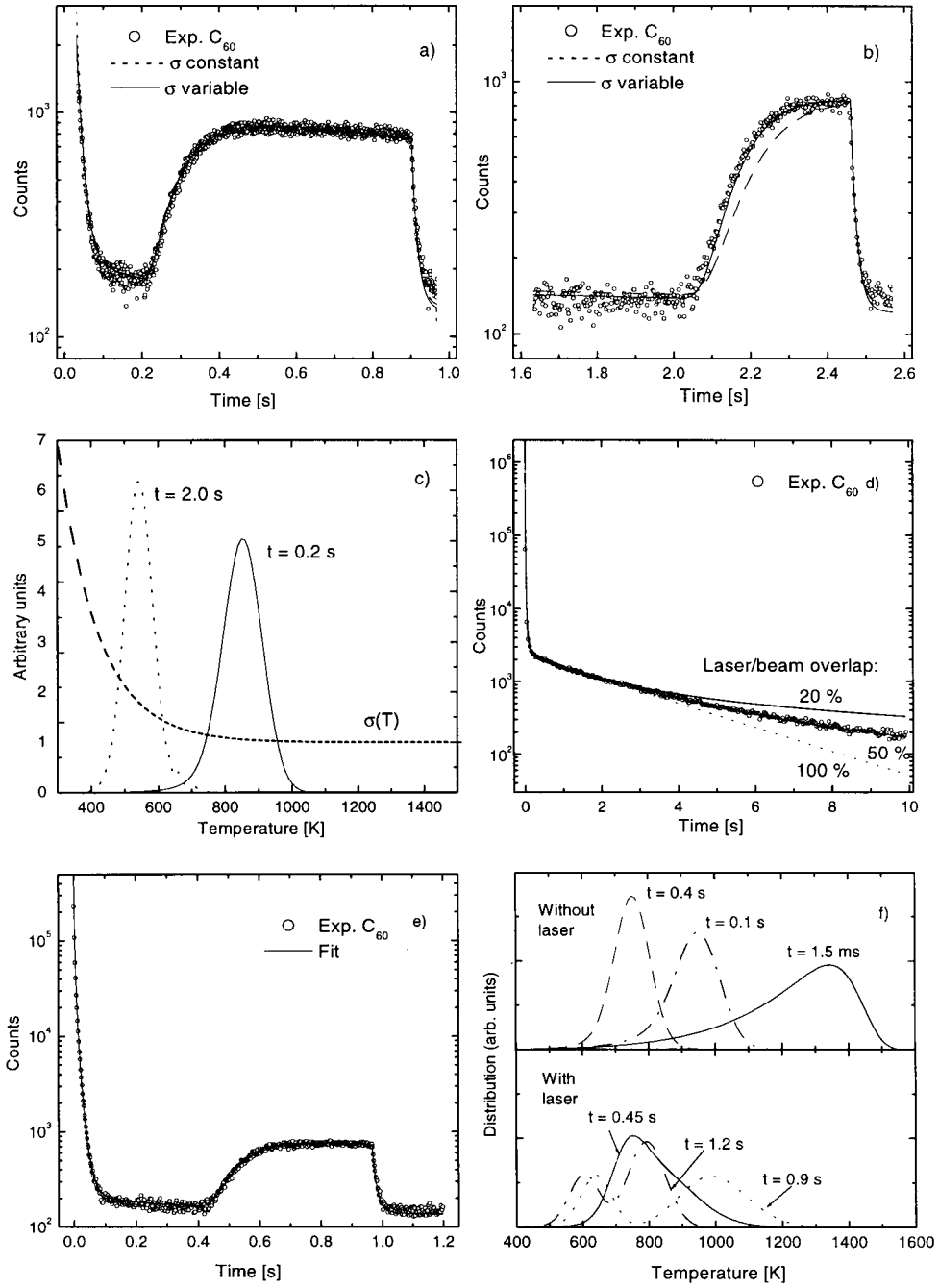

Fig. 11. Measurements for C_{60}^- ions in ASTRID irradiated with a Nd:YAG laser. In Figure 11a the laser was switched on 0.2 s after beam injection into the ring, and the laser beam was blocked after 0.9 s, and in Figure 11b the laser was on from 2.0 s to 2.45 s after injection. The solid lines represent simulations with the temperature dependent absorption cross-section illustrated in Figure 11c, which also shows the temperature distributions of the stored molecules at the times of laser on-set. The laser beam does not illuminate the ions uniformly, as the measurement in Figure 11d illustrates. Here the laser beam was on all the time, and the data are fitted well for overlap with 50% of the ions. Figure 11f shows the temperature distribution as a function of time in the simulation producing the fit to the measurement in Figure 11e.

intensity of the upper line is about a factor of two higher than estimated from the measured absorption strength [40–43]. The low-energy radiation is nearly two orders of magnitude stronger than the calculated contribution from vibrations [26]. A similar result is obtained for C_{70}^- where the single-electron line at 0.9 eV dominates the absorption below about 1.3 eV [38,44]. The measured decay curve is reproduced with two lines at 0.9 eV and 0.25 eV with intensities of 650 eV/s and 210 eV/s at 1 500 K. The prediction from the measured absorption strength at 0.9 eV is estimated in Appendix C to be about 400 eV/s, and the calculated intensity from infrared-active vibrations is less than 10 eV/s [26].

5.1 CW-laser experiments

For a stored C_{60}^- beam, the molecules can be heated by absorption of 1.16 eV photons from a Nd:YAG laser. Figure 11 shows the results of measurements of this type at ASTRID. In the first two cases, the laser was turned on after the signal from thermionic emission had been quenched by radiative cooling and at different time delays after injection of the ion beam. The thermionic emission is then regenerated, and after a short time a nearly stationary situation is established with an equilibrium between heating and cooling. When the laser is turned off, the neutrals yield again falls rapidly to the level

corresponding to collisional detachment alone. As illustrated by the curve in Figure 11a, the simulation can describe also this situation, with the cooling parameters determined by a fit to the experiment without laser heating. This gives important support to the interpretation of our electron emission measurements in terms of radiative cooling.

Laser heating at long delays after ion injection gives information about the dynamics at lower temperatures that cannot be obtained from the simple lifetime experiments. In order to fit the measurement in Figure 11b with the same parameters it is seen to be necessary to include a temperature dependence of the photon-absorption cross-section, as illustrated in Figure 11c. Such a dependence is expected since the laser frequency is very close to the centre of the absorption line of the additional electron in C_{60}^- and this line is strongly broadened at high temperatures [38]. If the integral of the line is constant, the absorption at the centre is weaker at high temperatures. With the curve shown in Figure 11c the measurement is reproduced but we do not have sufficient data to establish the shape of the curve in detail. In the analysis of measurements extending to several seconds after beam injection it is important to include the reduction of the heat capacity at low temperatures (Fig. 5) and also the vibrational cooling (see Appendix B).

Figure 11d shows a fit to the measurement with the laser on all the time, illustrated also in Figure 3. With a constant and uniform laser illumination, an equilibrium distribution in temperature should be approached, and the signal should decrease exponentially. The deviation at long times from exponential decay therefore indicates an incomplete overlap of the laser beam with the beam of stored ions. The three calculations shown in Figure 11d correspond to the same power absorbed at short times but by different fractions of the ions. The experimental results are reproduced when about half of the beam is unaffected by the laser. The overlap was stable after alignment of the two beams but varied somewhat between different series of measurements. Of course the division of the ions into fractions with zero and 100% overlap is a crude approximation, but the experiment is not sensitive to details of the laser intensity distribution.

A measurement with the laser beam on from 0.4 to 1.0 s and the corresponding simulation are illustrated in Figures 11e and 11f. The distribution at 1.5 ms after ion exit from the source corresponds approximately to the first point on the measured yield curve, and the distribution is cut off at $\sim$ 1 500 K by depletion due to thermionic emission. Before the laser is turned on, the distribution moves down in temperature due to radiative cooling and it narrows owing to the strong decrease in cooling with decreasing temperature. In the calculation of the laser heating, the inhomogeneous overlap between the laser and ion beams is represented by a separation of the beam into two components with and without heating. Part of the distribution therefore continues to cool down while another part is reheated and reaches an equilibrium while the laser is on.

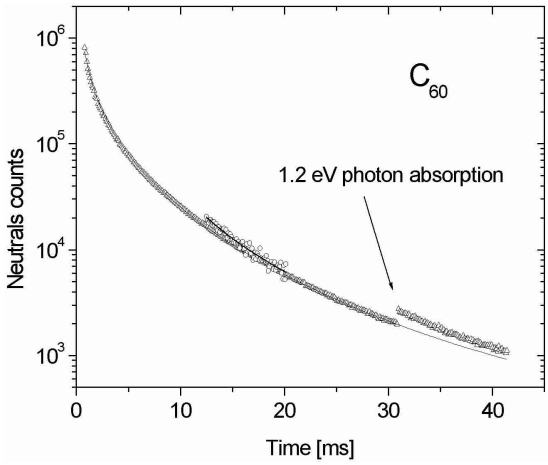

Fig. 12. Measurement with C_{60}^- stored in ELISA and exposed to a 2 mJ laser pulse of 1.2 eV photons at 30.3 ms after injection ($\triangle$). The line through the triangles is a fit with the analytical function given in reference [11]. The circles and the line through these points are discussed in the text (see Eq. (25)).

5.2 Pulsed-laser experiments

The analysis of the experiment with the pulsed laser is illustrated in Figure 12. The triangles show a spectrum for stored C_{60}^- ions, similar to Figure 9c except for the increase in yield after irradiation with a laser pulse at 30.3 ms. Each point in the spectrum corresponds to a sum over one revolution time (see Fig. 4). The curve through the points was obtained from simulation of a spectrum without a laser pulse with the simple analytical expression given in reference [11], with parameters values very close to those given there. From this simulation we obtain the variation with time of the internal temperature in the continuous-cooling model (Eq. (9)). According to our interpretation, the increase in the yield after 30.3 ms is due to heating by absorption of a 1.2 eV photon. The ions which have absorbed a photon should, so to speak, be translated back in time to the moment when their internal energy was larger by 1.2 eV.

We have checked the consistency of this description by the following analysis: we assume that the number of absorbed photons follows a Poisson distribution. Accordingly, the yield in the five highest channels in a period at time t (see Fig. 4), renormalised by a factor 3.8 to correspond to the counts in a full revolution, was expressed as

$$Y(t) = (Y_0(t) + aY_0(t - \delta t_1) + (a^2/2)Y_0(t - \delta t_2) + ...)\mathrm{e}^{-a}, \quad (24)$$

where $Y_0(t)$ is the decay curve without the laser pulse and a is the probability for absorption of a single photon, while $-\delta t_n$ is the shift back in time from 30.3 ms corresponding to an increase of the internal energy by $n \times 1.2$ eV. If only the first-order term is included, there are only two parameters in this expression, a and δt_1. They can be determined by the requirement that both the absolute magnitude of $Y(t)$ and its logarithmic slope should be reproduced. However, it is necessary also to include the second-order term

in equation (24). The additional parameter δt_2 was chosen to give the correct ratio $Y_0(t-\delta t_2)/Y_0(t-\delta t_1)$ according to the Arrhenius expression in equation (A.2). Note that it is only for this evaluation of the small second-order term that the temperature development in equation (9), determined from the simulation, is used. The contribution from absorption of three photons can be estimated in the same way and it turns out to be negligible.

The analysis is illustrated in Figure 12. When only absorption of up to two photons is included, we obtain from equation (24)

$$(Y(t)-Y_0(t)\mathrm{e}^{-a})/a = (Y_0(t-\delta t_1) + (a/2)Y_0(t-\delta t_2))\mathrm{e}^{-a}. \quad (25)$$

This equation expresses more directly the idea that the additional yield after photon absorption corresponds to the yield at earlier times. The circles in Figure 12 indicate values of the left hand side of equation (25), with $a = 0.13$ and plotted at $t - \delta t_1$ with $\delta t_1 = 18.5$ ms. The points are compared with a curve representing the right hand side of equation (25), and the values of a and δt_1 have been chosen to give optimal agreement with this curve. For fixed δt_1, the value of a can be chosen to bring the average magnitude into agreement with the curve, and δt_1 has been chosen to bring the slopes into agreement. For larger values of δt_1, the slope of the curve is too steep, and for smaller values it is too flat. According to the temperature evolution given by equation (9), $\delta t_1 = 18.5$ ms corresponds to a change in internal energy which is very close to the photon energy of 1.2 eV, and this gives a (nearly) independent confirmation of the cooling analysis.

6 Conclusions

Together with our earlier experimental and theoretical investigations of fullerenes [11,12,26,28], the measurements presented here represent the most detailed study yet made of radiative cooling rates for clusters. Ion storage rings have turned out to be a unique tool for these investigations. The decay of cluster ions is easy to detect and can be followed over five orders of magnitude in time. Already in reference [11] it was established that the radiative cooling of C_{60} at temperatures above $\sim 1\,000$ K is dominated by electronic transitions. Similar results were obtained at about the same time for smaller molecules for which the radiation intensity could be calculated from known oscillator strengths of electronic transitions [20]. This approach has also been used to predict the heat radiation from C_{60} on the basis of data for absorption by C_{60} in solution and in solid films [27]. However, the absorption at low frequencies is very different in the two phases and this leads to differences by several orders of magnitude in predictions of the radiation intensity below $\sim 2\,000$ K [26].

For the magic fullerenes C_{60} and C_{70} the HOMO-LUMO gap is fairly large, and in the anions there is a strong absorption line in the gap from a transition of the additional electron. We have attempted to account for the cooling rates for C_{60}^- and C_{70}^- by the emission from this transition, calculated from absorption strengths measured for molecules in solution at room temperature. We find that the oscillator strengths of the lines have to be somewhat larger than the measured ones. Furthermore, to reproduce the temperature dependence of the cooling we must introduce emission at long wavelengths with an intensity which is more than an order of magnitude higher than that calculated for the infrared-active vibrations. The strong radiation at long wavelengths is probably associated with vibronic transitions and it indicates that at high temperatures there are efficient mechanisms for transfer of electronic oscillator strength to low- energy vibrational excitations.

These comparisons give a further illustration of the difficulties involved in basing estimates of radiation intensities on measured absorption cross-sections. The main problem is that the absorption has been measured in solution at low temperatures and it can be quite different in the gas phase at the high temperatures where the heat radiation is observed [28]. An alternative is to apply a dielectric model of fullerenes, as developed in reference [26]. Here the distribution of oscillator strength at low frequencies is determined as the tail of the plasmon resonances, and one may expect such a distribution to be approached at high temperatures, where the detailed quantum structure is washed out. The model reproduces the measured radiative cooling of nearly all the investigated fullerene anions to within a factor of two. This is quite a remarkable result since one might have expected the radiation to depend strongly on details of the low-energy spectrum of electronic transitions at the fairly low temperatures corresponding to electron emission from anions [26].

Can the results be extrapolated to neutral and positively charged fullerenes? As for anions, the closed-shell electronic structure is broken for positive ions, and the model predictions are expected to have a similar accuracy. For neutral molecules, the HOMO-LUMO gap is large and this should lead to lower intensities of thermal radiation. The observed slow cooling for C_{50}^- gives an indication of the magnitude of this reduction. Since neutral C_{60} and C_{70} molecules have larger HOMO-LUMO gaps than C_{50}, the intensity of thermal radiation from these molecules should be very low in the temperature range of our measurements, at least an order of magnitude lower than observed for the anions. We therefore now believe that the apparent good agreement [8,11] between our results for C_{60}^- and the estimate in reference [4] of radiation from neutral C_{60} molecules is fortuitous [26]. For the non-magic fullerenes with smaller HOMO-LUMO gaps, the single additional electron in the anions should be less important.

For both neutral and charged fullerenes, the accuracy of the model should be better at the high temperatures characteristic of C_2 emission, since here a gap of about 1 eV has a very small influence on the radiation intensity [26]. The model should therefore be useful for the analysis of experiments on C_2 evaporation, aiming at a determination of the C_2 binding energies [6–8]. The strong

temperature dependence of the radiation intensity may even be used to determine these binding energies from the cooling of ions in a storage ring [32] since, according to equation (14), the characteristic temperature for exponential quenching of the decay rate is proportional to E_b.

This work has been supported by the Danish National Research Foundation through the research centre ACAP (Aarhus Center for Atomic Physics), and by the EU Research Training Network, Contract HPRN-CT-2000-0002. It is a pleasure to acknowledge the cooperation of the staff of ISA (Institute for Storage Ring Facilities, Aarhus) in the experiments and the critical comments to the manuscript from E. Bonderup and from our referees.

Appendix A

In this appendix we discuss briefly the description of statistical electron emission. A more detailed discussion is given in reference [14]. With the assumption of a statistical equilibrium in the excited molecule and detailed balance symmetry between electron attachment and electron emission, one obtains for the emission rate constant,

$$k(E) \simeq \frac{m}{\pi^2\hbar^3}\langle\sigma_a\rangle_{T_\mathrm{f}}(k_\mathrm{B}T_\mathrm{f})^2\frac{g_\mathrm{f}}{g_\mathrm{i}}\frac{\rho(E-E_\mathrm{b})}{\rho(E)}\,. \qquad \text{(A.1)}$$

Here m is the electron mass and T_f is the temperature of the molecule after the emission. The average of the attachment cross-section σ_a contains a weighting by the electron kinetic energy and by a Boltzmann factor corresponding to the temperature T_f. The quantities g_f and g_i are degeneracy factors for the electron in the final and initial states ($g_\mathrm{f} = 2$), and the last factor is the ratio of the vibrational level densities of the molecule in these states. The frequency spectrum of vibrations is nearly the same in the two states, and hence the level densities can be represented by the same function ρ. We assume that the energy barrier E_b is equal to the electron affinity of the neutral molecule.

In order to express the rate constant in Arrhenius form, we expand the logarithm of the level density around the average energy $E - E_\mathrm{b}/2$. Combining all the factors in front of the level density ratio in equation (A.1) into a frequency ν, we then obtain [14,31],

$$k(E) = \nu\exp\left(-E_\mathrm{b}/k_\mathrm{B}T_\mathrm{e}\right), \qquad \text{(A.2)}$$

with an "emission temperature" given by

$$T_\mathrm{e} \simeq T - E_\mathrm{b}/2C. \qquad \text{(A.3)}$$

Here T is the temperature before emission, and the last term in equation (A.3) is the finite-heat-bath correction [45]. The most important parameter in equation (A.2) is the electron affinity, which is known fairly well for the fullerenes [15]. It depends only weakly on the number of atoms and in the first analysis we have assumed the value to be $E_\mathrm{b} = 3.15$ eV for all the fullerenes, except for the magic numbers $N = 60$ and 70 where accurate values of $E_\mathrm{b} = 2.67$ and 2.68 eV have been measured [46]. The weaker binding of an additional electron in these cases is connected to the high stability of the magic molecules. According to Figure 3 in reference [15], the electron affinity is also somewhat lower in the regions $N = 36$–40 and 62–68, and we have for these molecules used the value $E_\mathrm{b} = 2.85$ eV as an alternative (see also Ref. [47]). We estimate the uncertainty of E_b to be about $\pm 5\%$ for most of the other fullerenes.

According to equation (A.1), the factor ν is proportional to the cross-section for attachment of low-energy electrons. As discussed in reference [14], a cross-section of 60 Å^2, with an uncertainty of about 50%, appears to be a good approximation for C_{60}. For the other fullerenes we have scaled the cross-section with N. The degeneracy of the LUMO level occupied by the additional electron has been assumed to be $g_\mathrm{i} = 6$ for C_{60} and $g_\mathrm{i} = 2$ for the other fullerenes [39]. With these parameters, we obtain $\nu = 3 \times 10^6 (T_\mathrm{f}[\mathrm{K}])^2$ for emission from C_{60}^-. An uncertainty of a factor of two in ν is not very important in the analysis.

Appendix B

In this appendix we discuss briefly the thermal radiation from fullerenes. A more detailed discussion is given in references [14,26]. The interaction of fullerenes (mainly C_{60}) with radiation has been studied intensively since their discovery. In fact, the early interest in C_{60} was partly motivated by attempts to find the origin of absorption bands observed in radiation from space. Absorption in the visible and UV range has been studied mainly for C_{60} and C_{70} in solution and for solid films but also for these molecules in the gas phase. From detailed balance, one finds that the intensity of radiation from an isolated molecule with temperature T is related to the absorption cross-section as a function of temperature and frequency through

$$I_\mathrm{r}(T) = \frac{\hbar}{\pi^2 c^2}\int \mathrm{d}\omega\,\omega^3\sigma(T-\hbar\omega/C,\omega) \times \left[\exp\left(\hbar\omega/k_\mathrm{B}(T-\hbar\omega/2C)\right)-1\right]^{-1}. \qquad \text{(B.1)}$$

The absorption cross-section σ includes a reduction for stimulated emission, *i.e.*, it is determined by the net absorption, which is the quantity normally measured in experiments. In the weight function, the temperature is reduced by the correction for finite heat capacity, in analogy to equation (A.3) (see also Ref. [25]).

A few spectroscopic studies have been made of the emission of radiation from very hot fullerenes and they indicate that the emission is broad-band and quite similar to black-body radiation [21]. At high temperatures where the electronic degrees of freedom are not frozen, the radiation is dominated by the electrons because of their small mass. On the other hand, infrared emission from vibrations dominates at low temperatures, where the Boltzmann factors for electronic excitations become very small.

As argued in reference [11], our observation of cooling of stored C_{60}^- ions cannot be explained by infrared emission from vibrations. The temperature range of our

experiments, 1 000–1 500 K, is above the transition region where thermal radiation of electronic origin sets in. This transition has also been observed for smaller molecules, where the radiation intensity could be calculated from known oscillator strengths of electronic transitions [20]. A similar approach has been tried for the radiation from C_{60} [27], but such calculations are of limited scope for the fullerenes. The main reason is that there is strong electron-electron correlation and also coupling of electronic and vibrational transitions, especially at high temperatures. The electronic absorption of radiation is therefore not limited to narrow lines corresponding to well defined transitions between single- electron states, and the distribution of oscillator strength depends on the temperature [38,48]. In reference [26] the thermal radiation was instead estimated from a classical dielectric model of the electromagnetic response of a fullerene molecule, and we have mainly compared our measurements to predictions from this model. Such calculations also have the advantage that they give a general prediction for all the fullerene molecules. For most of these there is little information available on the detailed absorption spectrum.

The radiation power in equation (B.1) may be represented by the macroscopic black-body formula,

$$I_{\mathrm{r}} = S\sigma_0 a(T) T^4, \tag{B.2}$$

where S is the surface area, $\sigma_0 = 3.54 \times 10^{-9}$ eV s^{-1} Å^{-2} K^{-4} is the Stefan-Boltzmann constant, and the absorptivity $a(T)$ equals the absorption cross-section $\sigma(\omega)$ divided by the geometrical cross-section and averaged over the Planck spectrum of black-body radiation (with the small corrections in Eq. (A.3) for the finite heat capacity) [26]. The dielectric model predicts $\sigma(\omega) \propto \omega^2$ for small ω, and this implies $a(T) \propto T^2$ and $I_{\mathrm{r}} \propto T^6$. At 1 400 K the radiation intensity from a C_{60} molecule becomes $I_{\mathrm{r}} \approx 300$ eV/s and, with the scaling of parameters suggested in reference [26], the intensity is approximately proportional to the number of atoms N in a fullerene molecule. The model predicts an intensity of 3.3×10^4 eV/s for C_{60} at 3 000 K, a typical temperature for C_2 emission from fullerenes, and this is about 10% higher than obtained with an exact T^6 scaling from 1 400 K. For comparison, a value of $I_{\mathrm{r}} = 2{-}3 \times 10^4$ eV/s is obtained from the data in reference [6] for cationic fullerenes ($N < 60$). To derive this estimate, we have used a value $G = 33$ of the Gspann parameter and a temperature corresponding to $k_{\mathrm{B}}T = 0.3$ eV, and we have included the correction by a factor of three mentioned in reference [34].

At not too high temperatures, the dielectric model is expected to overestimate the thermal radiation due to the presence of a HOMO-LUMO gap, which blocks the emission of low energy photons (Fig. 9 in Ref. [26]). In neutral fullerene molecules, the gap is of order 1 eV but it varies strongly with N [38,47]. The trend of the variation seems to be that the gap is largest in the region $N = 60$–70. For ions there are additional electronic transitions available and the radiation is expected to be closer to the model prediction. We shall especially consider the influence of the additional electron in the anions of C_{50}, C_{60}, and C_{70}. The calculations in reference [39] predict that the lowest transition energy for this electron is highest in C_{50}, somewhat lower in C_{60}, and very small in C_{70}. For the latter two molecules, the transition energies and strengths have been determined in experiments [40–44], and the energies, 1.15 eV and 0.91 eV, follow the predicted trend. These two lines, with a strong thermal broadening, have also been observed for hot anions in a storage ring [38]. Spectroscopy in the energy range 0.7 to 3 eV on stored C_{50}^- ions did not reveal any strong absorption line but only the typical monotonic increase in absorption above ~ 1 eV. This indicates that the energy of the single-electron transition is probably above ~ 1.5 eV, where it may be hidden in the strong absorption lines for the neutral molecule.

The thermal radiation from infrared-active vibrations was also estimated in reference [26], with an upper limit of about 10 eV/s at 1 500 K for the fullerenes with lower symmetry. This is a low intensity compared to the observed cooling power. However, vibrations can still play an important role because of the strong coupling between vibrational and electronic transitions, which is reflected in the thermal broadening of electronic absorption lines [38, 48]. For example, vibrational transitions can "steal" oscillator strength from electronic transitions [49]. Our observations of radiative cooling may give information on the importance of such mechanisms. In the laser experiments with C_{60}^- the cooling at long times and fairly low temperatures is important and we have added to the electronic radiation a vibrational contribution given by equation (44) of reference [26].

Appendix C

In this appendix we estimate the intensities of thermal radiation from the single additional electron in C_{60}^- and C_{70}^-, based on equation (B.1) and measurements of absorption [40–44]. For C_{60}^- a line at 1 078 nm has been observed, with extinction coefficient 12 000 (ℓ/mol) cm^{-1}. To convert this into a molecular absorption cross-section σ_{m}, we divide by Avogadro's number and multiply by ln10, and we obtain $\sigma_{\mathrm{m}} = 0.46$ Å^2. For the integration in equation (B.1) we need also the relative width of the absorption peak which appears to be about 5% FWHM [42]. However, there are strong vibronic side bands at shorter wavelengths which increase the integrated cross-section by about a factor of two.

We may argue that the side bands should be included as additional oscillator strength at the unshifted line frequency ω_0: they appear because the equilibrium distance between carbon atoms is slightly different in the excited electronic state. In the sudden approximation, the probabilities for vibrational excitation can be calculated as the square of the matrix element of the shift operator $\delta(\partial/\partial x)$ between the initial and final vibrational states, where δ is the shift of the equilibrium value of the vibrational coordinate x. The symmetry of the matrix element then implies that the ratio of the probabilities for excitation and de-excitation equals the Boltzmann factor giving the relative

populations of the initial states for the two transitions. Observations of absorption at high temperatures T have confirmed this prediction of a skew line shape $\sigma(T,\omega)$, fulfilling the relation $\sigma(T,\omega_0+\Delta\omega)/\sigma(T,\omega_0-\Delta\omega) \simeq \exp(\hbar\Delta\omega/k_{\rm B}T)$ [38]. If we disregard the factor ω^3 in equation (B.1) and also unity in the Planck factor, the integral becomes just the integrated cross-section multiplied by the Boltzmann factor corresponding to frequency ω_0. Inclusion of the factor ω^3 in the integrand gives a factor close to ω_0^3.

With an effective linewidth of 10% when the sidebands are included, we obtain for the integrated cross-section, $\hbar\int\sigma{\rm d}\omega = 0.053$ eV Å^2. The Planck factor is $7\,290^{-1}$ at 1 500 K if the finite-heat-bath correction is omitted, and this correction gives a reduction by a factor 0.78. We must also take into account the polarisation of the solvent with refractive index $n \simeq 1.4$, and this adds a factor of $9n/(n^2+2)^2 = 0.79$ to our estimate of $I_{\rm r}$ [28]. Finally, we then arrive at an estimate of the radiation intensity in equation (18), $I_{\rm r} \simeq 200$ eV/s at 1 500 K, from the single-electron transition at 1.15 eV in C_{60}^-.

A similar estimate can be made for C_{70}^-, based on the measurement in reference [44] of absorption in solution. The line is found to be close to 0.9 eV, with a maximum extinction coefficient of 4 000 (ℓ/mol) cm^{-1} and apparently with a Lorentzian line shape with $\Gamma/\hbar\omega_0 \sim 10\%$. The Planck factor is $1\,110^{-1}$ with an additional factor of 0.87 for the finite-heat-bath correction. We take the correction for refraction to be a factor 0.79 as above. We then arrive at the estimate $I_{\rm r} \simeq 400$ eV/s at 1 500 K from the single-electron transition in C_{70}^-.

As discussed in Section 5, these estimates are somewhat lower than the radiation intensities needed to reproduce the observed cooling. One possible explanation is that, in addition to the effect associated with polarisation of the solvent, the surrounding solvent molecules could influence the tail of the wave function of the single additional electron in the fullerene anion and thereby modify the oscillator strength of the transition. This could be significant because of the drastic reduction in strength of low-energy transitions due to screening by electron polarisation in the fullerene molecule. The effect of screening has been demonstrated both by comparisons of quantum calculations with experiments [50] and in the development of a classical dielectric model [26]. In the latter calculations it was found necessary to introduce a spill-out of a small part of the density of loosely bound electrons in order to account for the measured absorption at low energies. Similarly, the tail of the wave function for the single electron is no doubt important. Such questions could be resolved by measurements of absorption in gas-phase molecules, for example with the method used in reference [38], but it is difficult to obtain absolute cross-sections.

References

1. H.W. Kroto, Nature **329**, 529 (1987).
2. R.E. Smalley, in *Atomic and Molecular Clusters*, edited by E.R. Bernstein (Elsevier, Amsterdam, 1990), Chap. 1.
3. R. Wörgötter, B. Dünser, P. Scheier, T.D. Märk, M. Foltin, C.E. Klots, J. Laskin, C. Lifshitz, J. Chem. Phys. **104**, 1225 (1996).
4. E. Kolodney, A. Budrevich, B. Tsipinyuk, Phys. Rev. Lett. **74**, 510 (1995).
5. K. Hansen, O. Echt, Phys. Rev. Lett. **78**, 2337 (1997).
6. K. Hansen, E.E.B. Campbell, J. Chem. Phys. **104**, 5012 (1996).
7. J. Laskin, C. Lifshitz, Chem. Phys. Lett. **277**, 564 (1997).
8. C. Lifshitz, Int. J. Mass Spectrom. **198**, 1 (2000).
9. C. Lifshitz, Chem. Soc. Rev. **30**, 186 (2001).
10. P. Hvelplund, Phys. Scripta **T59**, 244 (1995).
11. J.U. Andersen, C. Brink, P. Hvelplund, M.O. Larsson, B. Bech Nielsen, H. Shen, Phys. Rev. Lett. **77**, 3991 (1996).
12. J.U. Andersen, C. Brink, P. Hvelplund, M.O. Larsson, H. Shen, Z. Phys. D **40**, 365 (1997).
13. K. Hansen, J.U. Andersen, P. Hvelplund, S.P. Møller, U.V. Pedersen, V.V. Petrunin, Phys. Rev. Lett. **87**, 123401 (2001).
14. J.U. Andersen, E. Bonderup, K. Hansen, Review of thermionic emission from clusters, to appear in J. Phys. B.
15. O.V. Boltalina, I.N. Ioffe, L.N. Sidorov, S. Gotthard, K. Vietze, J. Am. Chem. Soc. **122**, 9747 (2000).
16. R.C. Dunbar, Mass Spectrom. Rev. **11**, 309 (1992).
17. R.C. Dunbar, J. Chem. Phys. **95**, 2537 (1991).
18. G.T. Uchi, R.C. Dunbar, J. Chem. Phys. **96**, 8897 (1992).
19. R.C. Dunbar, J. Phys. Chem. **98**, 8705 (1994).
20. P. Boissel, P. de Parseval, P. Marty, G. Lefèvre, J. Chem. Phys. **106**, 4973 (1997).
21. R. Mitzner, E.E.B. Campbell, J. Chem. Phys. **103**, 2445 (1995).
22. U. Frenzel, U. Hammer, H. Westje, D. Kreisle, Z. Phys. D **40**, 108 (1997).
23. C. Walther, G. Dietrich, W. Dostal, K. Hansen, S. Krückeberg, K. Lützenkirchen, L. Schweikhard, Phys. Rev. Lett. **83**, 3816 (1999).
24. C.F. Bohren, D.R. Huffman, *Absorption and Scattering of Light by Small Particles* (John Wiley, N.Y., 1983).
25. K. Hansen, E.E.B. Campbell, Phys. Rev. E **58**, 5477 (1998).
26. J.U. Andersen, E. Bonderup, Eur. Phys. J. D **11**, 413 (2000).
27. W.A. Chupka, C.E. Klots, Int. J. Mass Spectrom. Ion Proc. **167/168**, 595 (1997).
28. J.U. Andersen, E. Bonderup, Eur. Phys. J. D **11**, 435 (2000).
29. P. Hvelplund, J.U. Andersen, K. Hansen, in *Trapped Charged Particles and Fundamental Physics*, edited by D.H.E. Dubin, D. Schneider (AIP Conf. Proc. 457, N.Y. 1999), p. 220.
30. S.P. Møller, Nucl. Instrum. Meth. A **394**, 281 (1997).
31. J.U. Andersen, E. Bonderup, K. Hansen, J. Chem. Phys. **114**, 6518 (2001).
32. S. Tomita, J.U. Andersen, C. Gottrup, P. Hvelplund, U.V. Pedersen, Phys. Rev. Lett. **87**, 073401 (2001).
33. C.E. Klots, J. Chem. Phys. **92**, 5864 (1988).
34. The advantage of the present formulation is illustrated by an error in Appendix A of reference [6], where a similar model was applied. The second term in equation (A.4) should be omitted, and this leads to a reduction by a factor of three in equation (A.8).
35. J. Lindhard, V. Nielsen, Mat. Fys. Medd. Dan. Vid. Selsk. **38**, No. 9 (1971).

36. J.U. Andersen, E. Bonderup, E. Lægsgaard, A.H. Sørensen, Phys. Scripta **28**, 308 (1983).
37. H. Shen, C. Brink, P. Hvelplund, M.O. Larsson, Z. Phys. D **40**, 371 (1997).
38. K. Hansen, J.U. Andersen, H. Cederquist, C. Gottrup, P. Hvelplund, M.O. Larsson, V.V. Petrunin, H.T. Schmidt, Eur. Phys. J. D **9**, 351 (1999), and a continuation to be published.
39. S.J. Woo, E. Kim, Y.H. Lee, Phys. Rev. B **47**, 6721 (1993).
40. T. Kato, T. Kodama, T. Shida, Chem. Phys. Lett. **180**, 446 (1991).
41. M.A. Greaney, S.M. Gorun, J. Phys. Chem. **95**, 7142 (1991).
42. G.A. Heath, J.E. McGrady, R.L. Martin, J. Chem. Soc. Chem. Commun. (1992), p. 1272.
43. D.R. Lawson, D.L. Feldheim, C.A. Foss, P.K. Dorhout, C.M. Elliott, C.R. Martin, B. Parkinson, J. Electrochem. Soc. **139**, L68 (1992).
44. D.R. Lawson, D.L. Feldheim, C.A. Foss, P.K. Dorhout, C.M. Elliott, C.R. Martin, B. Parkinson, J. Phys. Chem. **96**, 7175 (1992).
45. C.E. Klots, Z. Phys. D **21**, 335 (1991), and references therein.
46. C. Brink, L.H. Andersen, P. Hvelplund, D. Mathur, J.D. Voldstad, Chem. Phys. Lett. **233**, 52 (1995).
47. H. Kietzmann, R. Rochow, G. Ganteför, W. Eberhardt, K. Vietze, G. Seifert, P.W. Fowler, Phys. Rev. Lett. **81**, 5378 (1998).
48. M.S. Hansen, J.M. Pacheco, G. Onida, Z. Phys. D **35**, 141 (1995).
49. M.J. Rice, H.-Y. Choi, Phys. Rev. B **45**, 10173 (1992).
50. G.F. Bertsch, A. Bulgac, D. Tománek, Y. Wang, Phys. Rev. Lett. **67**, 2690 (1991).